Quantum interference of ρ^0- and ω-mesons in the $\pi N \to e^+e^-N$ reaction

Matthias F. M. Lutz

GSI, Planckstrasse 1, D-64291 Darmstadt, Germany
Institut für Kernphysik, TU Darmstadt, D-64289 Darmstadt, Germany

Bengt Friman

GSI, Planckstrasse 1, D-64291 Darmstadt, Germany
Institut für Kernphysik, TU Darmstadt, D-64289 Darmstadt, Germany

Madeleine Soyeur

Département d'Astrophysique, de Physique des Particules,
de Physique Nucléaire et de l'Instrumentation Associée,
Service de Physique Nucléaire, CEA/Saclay,
F-91191 Gif-sur-Yvette Cedex, France

Abstract

The study of the $\pi N \to \rho^0 N$ and $\pi N \to \omega N$ amplitudes below and close to the vector meson production threshold ($1.4 < \sqrt{s} < 1.8$ GeV) reveals a rich structure arising from the presence of baryon resonances in this energy range. These resonances are reflected in the interference pattern of the e^+e^- decays of the ρ^0- and ω-mesons produced in π^-p and π^+n reactions. We discuss the shape and magnitude of the ρ^0-ω interference in the $\pi^-p \to e^+e^-n$ and $\pi^+n \to e^+e^-p$ reaction cross sections as functions of the total center of mass energy $\sqrt{s}$. We find contrasted results: the interference is largely destructive for the $\pi^-p \to e^+e^-n$ cross section but constructive for the $\pi^+n \to e^+e^-p$ cross section. An experimental study of these reactions would provide significant constraints on the coupling of vector meson-nucleon channels to low-lying baryon resonances.

Key words: Vector meson production; Baryon resonances; Dileptons; Quantum interference

PACS: 13.20; 13.75.G; 14.20.G

1 Introduction

Baryon resonances have been most extensively studied in partial-wave analyses of pion-nucleon elastic scattering data. Fairly accurate values of their masses, half-widths and pion-nucleon partial decay widths have been extracted up to pion-nucleon center of mass energies of about 2 GeV [1,2]. Isobar analyses of inelastic data ($\pi N \to \pi\pi N$) make it possible to study meson-nucleon final states other than πN, such as ρN and πN^* (where N^* denotes a low-lying baryon resonance which couples strongly to the πN channel) [3,4]. The $\pi N \to \pi\pi N$ data are known with much less statistical accuracy than the pion-nucleon elastic scattering data. For some partial waves, specific final states besides the πN and $\pi\pi N$ channels have to be included in the analyses to satisfy unitarity. The ηN channel in particular is needed at low energy for a proper description of the S_{11} wave [3,4]. Similarly, at higher energies, the ωN and $K\Lambda$ channels play a role [3,4].

The study of the $\pi^- p \to e^+e^-n$ and $\pi^+ n \to e^+e^-p$ processes described in this work aims at gaining understanding of the $\pi N \to \rho^0 N$ and $\pi N \to \omega N$ scattering amplitudes for center of mass energies close and below the vector meson production threshold ($1.5 < \sqrt{s} < 1.8$ GeV). There are well-known baryon resonances in this energy range, which contribute to the $\pi^- p \to e^+e^-n$ and $\pi^+ n \to e^+e^-p$ scattering amplitudes through their coupling to the $\rho^0 N$ and ωN channels. These amplitudes involve in addition significant non-resonant processes.

Phenomenological constraints on the ρNN^* and ωNN^* coupling strengths are useful both for baryon structure studies and for building models of vector meson propagation in the nuclear medium. On the one hand, it is of interest to compare the ρNN^* and ωNN^* coupling strengths entering the description of the $\pi^- p \to e^+e^-n$ and $\pi^+ n \to e^+e^-p$ cross sections to quark model predictions for the corresponding quantities. In particular, the e^+e^- channel offers the possibility to study the coupling of low-lying baryon resonances to the ωN channel below threshold. On the other hand, the ρNN^* and ωNN^* coupling strengths determine the contribution of resonance-hole states to the ρ^0- and ω-meson propagator in nuclear matter. It has been suggested that the spectral distribution of those mesons at high baryon density could be interpreted as a signal of chiral symmetry restoration in the nuclear medium [5] and hence be sensitive to the nonperturbative structure of Quantum Chromodynamics. The spectral functions of vector mesons in the nuclear medium should be reflected in the spectra of lepton pairs produced in photon- and hadron-nucleus reactions as well as in ultra-relativistic heavy ion collisions [6]. A proper understanding of the $\pi^- p \to e^+e^-n$ and $\pi^+ n \to e^+e^-p$ reactions appears as a first and necessary step towards a detailed interpretation of the production of lepton pairs off nuclei induced by charged pions. Because of the very large

width of ρ-mesons in nuclei, the production of e^+e^- pairs in pion-nucleus interactions is expected to be mostly sensitive to the in-medium propagation of ω-mesons for e^+e^- pair invariant masses close to vector meson masses [7,8]. Both the $\pi N \to e^+e^-N$ and $\pi A \to e^+e^-X$ cross sections could be measured at GSI-Darmstadt with the HADES detector [7,9].

The exclusive observation of neutral vector mesons through their e^+e^- decay presents definite advantages over their observation through final states involving pions. Firstly, there are no competing processes, such as $\pi\Delta$ production leading to the same final state and impairing the identification of the ρ-meson in the $\pi\pi N$ channel. Secondly, both the ρ^0- and ω-mesons decay into the e^+e^- channel. This leads to a quantum interference pattern which is expected to reflect the structure and relative sign of the $\pi N \to \rho^0 N$ and $\pi N \to \omega N$ scattering amplitudes. Such an interference in the e^+e^- channel, observed in the photoproduction of ρ^0- and ω-mesons at higher energies [10], has proved very useful in establishing the similarity of the $\gamma p \to \rho^0 p$ and the $\gamma p \to \omega p$ processes and the diffractive nature of these reactions for incident photon energies of a few GeV.

The $\pi N \to e^+e^-N$ cross section is connected to the $\pi N \to \rho^0 N$ and $\pi N \to \omega N$ scattering amplitudes by the Vector Meson Dominance assumption [11,12]. In this picture, the produced ρ^0- or ω-meson is converted into an intermediate time-like photon which subsequently materializes into an e^+e^- pair. The dynamics of the $\pi N \to e^+e^-N$, $\gamma N \to \pi N$ and $e^-N \to e^-\pi N$ processes is expected to be similar and dominated by the couplings of baryon resonances to the pion and to vector fields. In that sense, the study of the $\pi N \to e^+e^-N$ reaction complements programs devoted to the photo- and electroproduction of baryon resonances. There is presently a large activity in this field at ELSA [13], MAMI [14] and the Jefferson Laboratory [15].

To discuss the $\pi N \to e^+e^-N$ reaction, we use the $\pi N \to \rho^0 N$ and $\pi N \to \omega N$ amplitudes obtained in the recent unitary coupled-channel model of Ref. [16]. This is a relativistic approach where, in contrast to isobar analyses of πN scattering, the s- and d-wave pion-nucleon resonances are generated dynamically starting from an effective field theory of meson-nucleon scattering [16]. We present the model and its predictions for the $\pi N \to \rho^0 N$ and $\pi N \to \omega N$ amplitudes in Section 2. The calculation of the $\pi^- p \to e^+e^-n$ and $\pi^+ n \to e^+e^-p$ cross sections in the Vector Meson Dominance model is outlined in Section 3. Our numerical results for these cross sections are displayed in Section 4. We show how the $\rho^0 - \omega$ quantum interference pattern in the e^+e^- spectrum occurs in both isospin channels and evolves as function of the total pion-nucleon center of mass energy in the interval ($1.5 < \sqrt{s} < 1.8$ GeV). Concluding remarks are given in Section 5.

2 The $\pi N \to \rho^0 N$ and $\pi N \to \omega N$ amplitudes close to the vector meson production threshold

We describe the $\pi N \to e^+e^- N$ reaction for e^+e^- pair invariant masses ranging from $\sim$0.4 to $\sim$0.8 GeV. The exclusive measurement of the $e^+e^- N$ outgoing channel ensures that the e^+e^- pair comes from the decay of a time-like photon. In this respect, the identification of the e^+e^- decay of vector mesons is easier in the $\pi N \to e^+e^- N$ process than in the photoproduction reaction $\gamma N \to e^+e^- N$, where it interferes with Bethe-Heitler pair production. Assuming Vector Meson Dominance for the electromagnetic current [12], the $\pi N \to \rho^0 N$ and $\pi N \to \omega N$ amplitudes are the basic quantities entering the calculation of the $\pi N \to e^+e^- N$ cross section. At pion-nucleon center of mass energies close to the ρ^0- and ω-meson production threshold the kinetic energy of the particles in the entrance channel is large. Hence a relativistic description of the $\pi N \to \rho^0 N$ and $\pi N \to \omega N$ amplitudes is preferable.

We study the $\pi^- p \to e^+e^- n$ and $\pi^+ n \to e^+e^- p$ reactions in the framework of a recent relativistic and unitary coupled-channel approach to meson-nucleon scattering [16]. The available data on pion-nucleon elastic and inelastic scattering and on meson photoproduction off nucleon targets are fitted in the energy window $1.4 < \sqrt{s} < 1.8$ GeV, using an effective Lagrangian with quasi-local two-body meson-baryon interactions and a generalized form of Vector Meson Dominance to describe the coupling of vector mesons to real photons. The scheme involves the πN, $\pi\Delta$, ρN, ωN, $K\Lambda$, $K\Sigma$ and ηN hadronic channels, whose relevance in this energy range has been highlighted by earlier non-relativistic analyses [3,4]. The coupling constants entering the effective Lagrangian are parameters which are adjusted to reproduce the data. In view of the kinematics, only s-wave scattering in the ρN and ωN channels is included, restricting πN and $\pi\Delta$ scattering to s- and d-waves. The pion-nucleon resonances in the S_{11}, S_{31}, D_{13} and D_{33} partial waves are generated dynamically by solving Bethe-Salpeter equations [16].

The model provides a good fit to the $\pi^- p \to \rho^0 n$, $\pi^- p \to \omega n$ and $\gamma p \to \rho^0 p$ cross sections for $\sqrt{s} \leq 1.75$ GeV, where enough data close to threshold are available for comparison [16]. Above threshold, where higher partial waves should become important (in channels where pion-exchange effects are expected to be large), it underestimates significantly the $\pi^- p \to \rho^0 n$ and the $\gamma p \to \omega p$ cross sections. The model reproduces satisfactorily the πN scattering data (phase shifts and inelasticities) and pion photoproduction multipole amplitudes below the vector meson production threshold [16]. Our approach is therefore appropriate to values of $\sqrt{s} \leq 1.75$ GeV. In the $\rho^0 N$- and ωN-channels, the restriction to s-wave scattering means that the model applies to situations where the vector meson is basically at rest with respect to the scattered nucleon ($\sqrt{s} \simeq M_N + M_V$), where M_N and M_V denote the nucleon and

the vector-meson masses respectively. This assumption implies that the range of validity of the present calculation is limited to e^+e^- pairs with invariant masses $m_{e^+e^-}$ close to $(\sqrt{s} - M_N)$.

The $\pi N \to \rho N$ and $\pi N \to \omega N$ amplitudes are represented diagrammatically in Fig. 1. The $\pi N \to \rho N$ amplitude has isospin 1/2 and isospin 3/2 components while the $\pi N \to \omega N$ amplitude selects the isospin 1/2 channel. Both amplitudes have spin 1/2 and spin 3/2 parts.

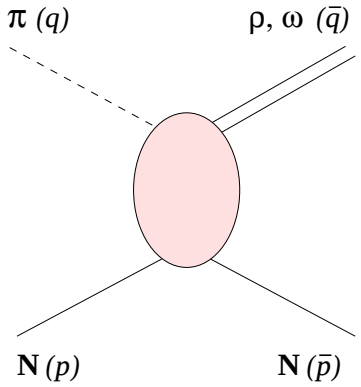

Fig. 1. The $\pi N \to \rho(\omega) N$ amplitude.

The invariant transition matrix elements for the $\pi N \to \rho N$ and $\pi N \to \omega N$ reactions are given by

$$\begin{aligned} &\langle \rho^j(\overline{q})\, N(\overline{p})|\, \mathcal{T}\, |\pi^i(q)\, N(p)\rangle \\ &\qquad = (2\pi)^4\, \delta^4(q + p - \overline{q} - \overline{p})\, \overline{u}(\overline{p})\, \epsilon^\mu(\overline{q})\, T^{ij}_{(\pi N \to \rho N)\,\mu}\, u(p), \end{aligned} \tag{1}$$

$$\begin{aligned} &\langle \omega(\overline{q})\, N(\overline{p})|\, \mathcal{T}\, |\pi^i(q)\, N(p)\rangle \\ &\qquad = (2\pi)^4\, \delta^4(q + p - \overline{q} - \overline{p})\, \overline{u}(\overline{p})\, \epsilon^\mu(\overline{q})\, T^{i}_{(\pi N \to \omega N)\,\mu}\, u(p), \end{aligned} \tag{2}$$

where $T^{ij}_{(\pi N \to \rho N)\,\mu}$ and $T^{i}_{(\pi N \to \omega N)\,\mu}$ are functions of the three kinematic variables $w = p + q = \overline{p} + \overline{q}$ $(\sqrt{w^2} = \sqrt{s})$, q and $\overline{q}$.

These scattering amplitudes can be decomposed into isospin invariant components as [17]

$$T^{ij}_{(\pi N \to \rho N)\,\mu}(\overline{q}, q; w) = \sum_I T^{(I)}_{(\pi N \to \rho N)\,\mu}(\overline{q}, q; w)\, P^{(I)\,ij}_{(\rho)}, \tag{3}$$

$$T^{i}_{(\pi N\to\omega N)\,\mu}(\overline{q},q;w) \;=\sum_{I} T^{(I)}_{(\pi N\to\omega N)\,\mu}\,(\overline{q},q;w)P^{(I)\,i}_{(\omega)}, \tag{4}$$

in which the isospin projectors are given for the $\pi N \to \rho N$ transition by

$$P^{(I=\frac{1}{2})\,i,j}_{(\rho)} \;=\; \frac{1}{3}\,\tau^{i}\tau^{j}, \tag{5}$$

$$P^{(I=\frac{3}{2})\,i,j}_{(\rho)} \;=\; \delta^{ij} - \frac{1}{3}\,\tau^{i}\tau^{j}, \tag{6}$$

and for the $\pi N \to \omega N$ transition by

$$P^{(I=\frac{1}{2})\,i}_{(\omega)} \;=\; \frac{1}{\sqrt{3}}\,\tau^{i}. \tag{7}$$

The isospin invariant amplitudes can be expanded further into components of total angular momentum using the relativistic projection operators introduced in Ref. [17]. Because our model is restricted to s-wave vector-meson nucleon final states, this expansion takes the simple form,

$$\begin{aligned} T^{(I)}_{(\pi N\to VN)\,\mu}(\overline{q},q;w) \;=&\; M^{(I,J=\frac{1}{2})}_{\pi N\to VN}(s)\; Y_{(J=\frac{1}{2})\,\mu}(\overline{q},q;w) \\ &+ M^{(I,J=\frac{3}{2})}_{\pi N\to VN}(s)\; Y_{(J=\frac{3}{2})\,\mu}(\overline{q},q;w), \end{aligned} \tag{8}$$

where V stands for ρ or ω and the angular momentum projectors are defined by [16]

$$Y_{(J=\frac{1}{2})\,\mu}(\overline{q},q;w) \;=\; -\frac{1}{2\sqrt{3}}\,(\gamma_{\mu} - \frac{w_{\mu}}{w^{2}}\,\not{w})(1 - \frac{\not{w}}{\sqrt{w^{2}}})\,i\gamma_{5}\,, \tag{9}$$

$$\begin{aligned} Y_{(J=\frac{3}{2})\,\mu}\;(\overline{q},q;w) \;=&\; -\frac{\sqrt{3}}{2}\,(1 + \frac{\not{w}}{\sqrt{w^{2}}})(q_{\mu} - \frac{w.q}{w^{2}}w_{\mu})\,i\gamma_{5} \\ &+\frac{1}{2\sqrt{3}}\,(\gamma_{\mu} - \frac{w_{\mu}}{w^{2}}\,\not{w})\,(1 - \frac{\not{w}}{\sqrt{w^{2}}})\,(\not{q} - \frac{w.q}{w^{2}}\,\not{w})\,i\gamma_{5}. \end{aligned} \tag{10}$$

In the more general notation of Ref. [16], the quantities defined by Eqs. (9) and (10) are written as $[Y^{(+)}_{0,\mu}(\overline{q},q;w)]_{13}$ and $[Y^{(-)}_{1,\mu}(\overline{q},q;w)]_{13}$ respectively.

In the center of mass system ($\vec{q}=-\vec{p}$), the time component of the spin projectors $Y_{(J=\frac{1}{2})\,\mu}$ and $Y_{(J=\frac{3}{2})\,\mu}$ vanishes and the space components read simply

$$Y_{(J=\frac{1}{2})\,j} \;=\; \frac{i}{\sqrt{3}} \begin{pmatrix} \sigma_j & 0 \\ 0 & 0 \end{pmatrix}, \tag{11}$$

$$Y_{(J=\frac{3}{2})\,j} \;=\; i\sqrt{3}\,p_j \begin{pmatrix} 0 & 1 \\ 0 & 0 \end{pmatrix} - \frac{i}{\sqrt{3}} \begin{pmatrix} 0 & \sigma_j(\vec{\sigma}.\vec{p}) \\ 0 & 0 \end{pmatrix}. \tag{12}$$

In these coordinates, the matrix elements of the spin projectors acting on Dirac spinors can be expressed in terms of Pauli spinors χ as

$$\overline{u}(\overline{p},\overline{\lambda})Y_{(J=\frac{1}{2})\,j}\,u(p,\lambda) \;=\; i\frac{\sqrt{p^0+M_N}\,\sqrt{\overline{p}^0+M_N}}{2\sqrt{3}M_N}\;\overline{\chi}(\overline{\lambda})\,\sigma_j\,\chi(\lambda), \tag{13}$$

$$\begin{aligned}\overline{u}(\overline{p},\overline{\lambda})Y_{(J=\frac{3}{2})\,j}\,u(p,\lambda) \;=\; & \frac{i\sqrt{3}}{2}\,\frac{\sqrt{\overline{p}^0+M_N}}{\sqrt{p^0+M_N}}\;\overline{\chi}(\overline{\lambda})\,\frac{(\vec{\sigma}.\vec{p})}{M_N}\,\frac{p^j}{m_\pi}\,\chi(\lambda) \\ & -\frac{i}{2\sqrt{3}}\,\frac{\sqrt{\overline{p}^0+M_N}}{\sqrt{p^0+M_N}}\,\frac{\vec{p}^{\,2}}{M_N}\;\overline{\chi}(\overline{\lambda})\,\sigma^j\,\chi(\lambda),\end{aligned} \tag{14}$$

where λ and $\overline{\lambda}$ are the polarizations of the ingoing and outgoing nucleons while p^0 and $\overline{p}^0$ are defined by $p^0=\sqrt{M_N^2+\overrightarrow{p}^{\,2}}$ and $\overline{p}^0=\sqrt{M_N^2+\overrightarrow{\overline{p}}^{\,2}}$. The $\pi N \to \rho N$ and $\pi N \to \omega N$ amplitudes in the S_{11}, S_{31}, D_{13} and D_{33} channels obtained in Ref. [16] are displayed in Figs. 2 and 3. The quantities shown are the amplitudes $M^{(I,J)}_{\pi N\to\rho N}(s)$ and $M^{(I,J)}_{\pi N\to\omega N}(s)$ defined by Eq. (8), which depend only on the center of mass energy $\sqrt{s}$. The coupling to subthreshold resonances is clearly exhibited in these pictures.

In the S_{11} channel, the N(1535) and the N(1650) resonances lead to peak structures in the imaginary parts of the amplitudes. The pion-induced ω production amplitudes in the D_{13} channel reflect the strong coupling of the N(1520) resonance to the ωN channel. The $\pi N \to \omega N$ amplitudes contain also significant contributions from non-resonant, background terms. We refer to [16] for a detailed discussion of the dynamical structure of the amplitudes and for the comparison to quark-model coupling constants of the effective coupling strengths of the vector meson-nucleon channels to the baryon resonances contributing to the amplitudes.

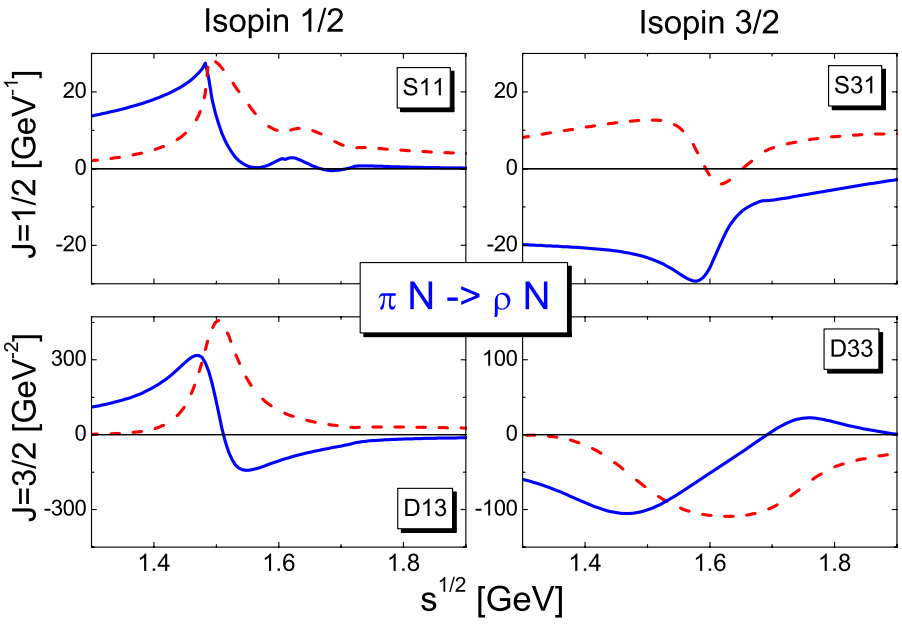

Fig. 2. Real and imaginary parts of the $\pi N \to \rho^0 N$ amplitudes in the pion-nucleon S_{11}, S_{31}, D_{13} and D_{33} partial waves [16].

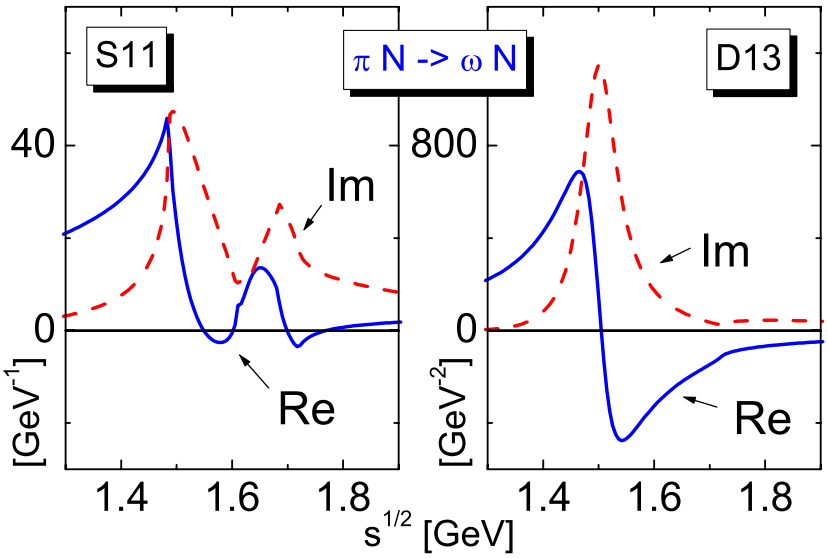

Fig. 3. Real and imaginary parts of the $\pi N \to \omega N$ amplitudes in the pion-nucleon S_{11} and D_{13} partial waves [16].

The $\pi^- p \to \rho^0 n$ and $\pi^- p \to \omega n$ amplitudes are obtained from the isospin 1/2 and isospin 3/2 scattering amplitudes by the relations,

$$M^J_{\pi^- p \to \rho^0 n} = -\frac{\sqrt{2}}{3} M^{(1/2,J)}_{\pi N \to \rho N} + \frac{\sqrt{2}}{3} M^{(3/2,J)}_{\pi N \to \rho N}, \tag{15}$$

$$M^J_{\pi^- p \to \omega n} = \sqrt{\frac{2}{3}} M^{(1/2,J)}_{\pi N \to \omega N}. \tag{16}$$

Similarly the $\pi^+ n \to \rho^0 p$ and $\pi^+ n \to \omega p$ amplitudes are given by

$$M^J_{\pi^+ n \to \rho^0 p} = \frac{\sqrt{2}}{3} M^{(1/2,J)}_{\pi N \to \rho N} - \frac{\sqrt{2}}{3} M^{(3/2,J)}_{\pi N \to \rho N}, \tag{17}$$

$$M^J_{\pi^+ n \to \omega p} = \sqrt{\frac{2}{3}} M^{(1/2,J)}_{\pi N \to \omega N}. \tag{18}$$

The quantities $M^J_{\pi^- p \to \rho^0 n}$ and $M^J_{\pi^- p \to \omega n}$ are displayed in Fig. 4. Their counterparts for the other reactions, $M^J_{\pi^+ n \to \rho^0 p}$ and $M^J_{\pi^+ n \to \omega p}$, are shown in Fig. 5.

The phases of the isospin coefficients appearing in Eqs. (15) and (17) play a crucial role in determining the $\rho^0 - \omega$ interference in the $\pi^- p \to e^+ e^- n$ and $\pi^+ n \to e^+ e^- p$ reaction cross sections. The real and imaginary parts of the $\pi^- p \to \omega n$ and of the $\pi^+ n \to \omega p$ amplitudes are the same and mostly positive. In contrast, the $\pi^- p \to \rho^0 n$ and $\pi^+ n \to \rho^0 p$ amplitudes have opposite signs. The $\pi^- p \to \rho^0 n$ amplitudes are predominantly negative and will therefore interfere destructively with the $\pi^- p \to \omega n$ amplitudes. The $\pi^+ n \to \rho^0 p$ and $\pi^+ n \to \omega p$ amplitudes have the same sign over a large $\sqrt{s}$ interval, leading to a constructive interference.

From Figs. 4 and 5, we expect the $\pi^- p \to e^+ e^- n$ and $\pi^+ n \to e^+ e^- p$ reaction cross sections to be very sensitive to the presence of baryon resonances below the vector meson production threshold.

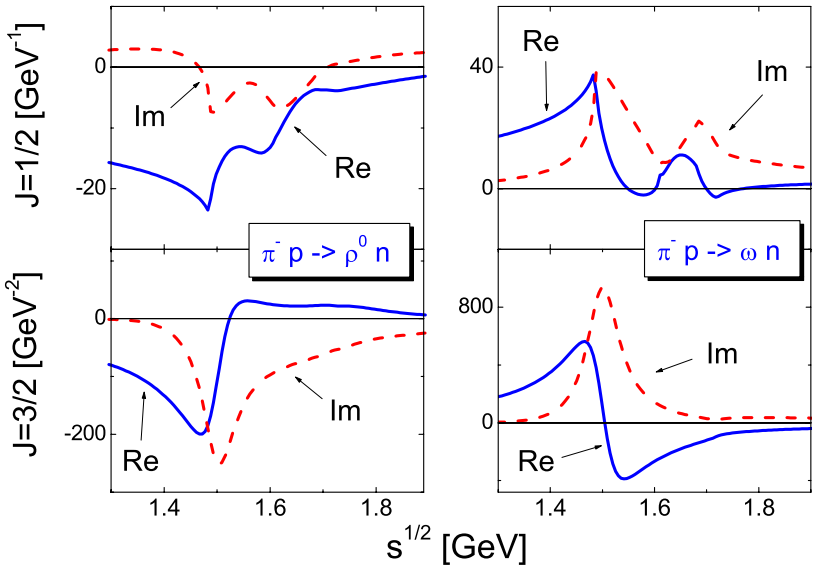

Fig. 4. Scattering amplitudes $M^J_{\pi^- p \to \rho^0 n}$ and $M^J_{\pi^- p \to \omega n}$ obtained from the model of Ref. [16] for the spin J=1/2 and J=3/2 channels.

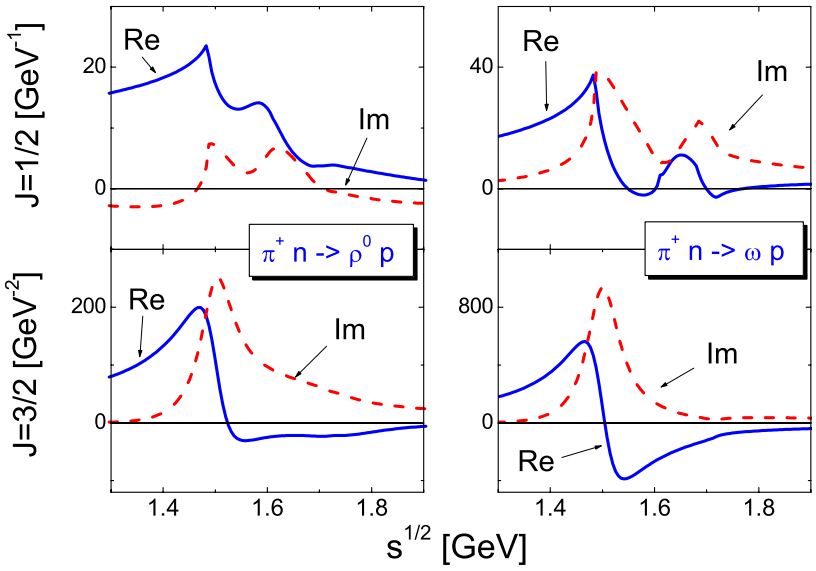

Fig. 5. Scattering amplitudes $M^J_{\pi^+ n \to \rho^0 p}$ and $M^J_{\pi^+ n \to \omega p}$ obtained from the model of Ref. [16] for the spin J=1/2 and J=3/2 channels.

3 Calculation of the $\pi^- p \to e^+ e^- n$ and $\pi^+ n \to e^+ e^- p$ cross sections close to the vector meson production threshold

The $\pi^- p \to e^+ e^- n$ and $\pi^+ n \to e^+ e^- p$ cross sections are calculated from the $\pi^- p \to \rho^0 n$, $\pi^- p \to \omega n$, $\pi^+ n \to \rho^0 p$ and $\pi^+ n \to \omega p$ amplitudes presented in Section 2, supplemented with the assumption of the Vector Meson Dominance of the electromagnetic current [11,12]. This assumption can be enforced in the effective Lagrangian by introducing vector meson-photon interaction terms of the form,

$$\mathcal{L}_{\gamma V}^{int} = \frac{f_\rho}{2M_\rho^2} F^{\mu\nu}\, \rho^0_{\mu\nu} \; + \; \frac{f_\omega}{2M_\omega^2} F^{\mu\nu}\, \omega_{\mu\nu}, \tag{19}$$

where the photon and vector meson field tensors are defined by

$$F^{\mu\nu} \; = \; \partial^\mu A^\nu - \partial^\nu A^\mu, \tag{20}$$

$$V^{\mu\nu} \; = \; \partial^\mu V^\nu - \partial^\nu V^\mu. \tag{21}$$

In equation (19), M_ρ and M_ω are the ρ- and ω-masses and f_ρ and f_ω are dimensional coupling constants. Their magnitude can be determined from the e^+e^- partial decay widths of the ρ- and ω-mesons to be [18]

$$|f_\rho| = 0.036\, GeV^2, \tag{22}$$

$$|f_\omega| = 0.011\, GeV^2. \tag{23}$$

The relative sign of f_ρ and f_ω is fixed by vector meson photoproduction amplitudes [16]. We assume that the phase correlation between isoscalar and isovector currents is identical for real and virtual photons as in Sakurai's realization of the Vector Meson Dominance assumption [11]. With the conventions used in this paper, both f_ρ and f_ω are positive. The form of the coupling terms of Eq. (19) is appropriate for describing the hadronic structure of massive photons.

We consider first the $\pi^- p \to e^+ e^- n$ reaction. The diagrams contributing to this process in the Vector Meson Dominance model are shown in Fig. 6.

We denote the momenta of the ingoing and outgoing hadrons as in Fig. 1 and the 4-momenta of the electron and the positron by $p_- = (p_-^0, \vec{p}_-)$ and

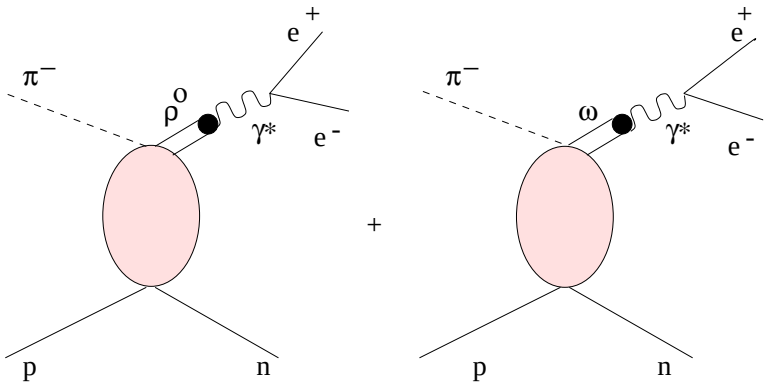

Fig. 6. Diagrams contributing to the $\pi^- p \to e^+ e^- n$ amplitude with intermediate ρ^0- and ω-mesons.

$p_+ = (p^0_+, \vec{p}_+)$ respectively. The differential cross section for the $\pi^- p \to e^+ e^- n$ reaction in the center of mass reference frame is then given by

$$\Big[\frac{d\sigma}{d\overline{q}^2}\Big]_{\pi^- p \to e^+ e^- n} = \frac{M_p\, M_n}{16\pi^2 s}\,\frac{|\vec{\overline{p}}|}{|\vec{p}|}\int \frac{d^3\vec{p}_+}{(2\pi)^3}\,\frac{m_e}{p^0_+}\int \frac{d^3\vec{p}_-}{(2\pi)^3}\,\frac{m_e}{p^0_-}\,(2\pi)^4$$
$$\sum_{\lambda,\overline{\lambda},\lambda_+,\lambda_-} \left|\mathcal{M}_{\pi^- p \to e^+ e^- n}(q,p,\lambda;p_+,\lambda_+,p_-,\lambda_-,\overline{p},\overline{\lambda})\right|^2 \delta^4(\overline{q}-p_+-p_-), \quad (24)$$

in which m_e denotes the electron mass and where the magnitude of the initial and final nucleon momenta is given as function of $\sqrt{s}$ and $\overline{q}^2$ by

$$|\vec{p}| \;=\; \frac{\sqrt{s}}{2}\Big[1 - 2\,\frac{M_p^2 + m_\pi^2}{s} + \frac{(M_p^2 - m_\pi^2)^2}{s^2}\Big]^{\frac{1}{2}}, \quad (25)$$

$$|\vec{\overline{p}}| \;=\; \frac{\sqrt{s}}{2}\Big[1 - 2\,\frac{M_p^2 + \overline{q}^2}{s} + \frac{(M_p^2 - \overline{q}^2)^2}{s^2}\Big]^{\frac{1}{2}}. \quad (26)$$

.

We factorize the invariant matrix elements into vector meson production and e^+e^- decay amplitudes as

$$\mathcal{M}_{\pi^- p \to e^+ e^- n}(q,p,\lambda;p_+,\lambda_+,p_-,\lambda_-,\overline{p},\overline{\lambda}) \;=$$
$$\mathcal{M}^{\mu}_{\pi^- p \to \rho^0 n}(q,p,\lambda;\overline{q},\overline{p},\overline{\lambda})\,\mathcal{M}_{\rho^0 \to e^+e^-\;\mu}(\overline{q};p_+,\lambda_+,p_-,\lambda_-)$$
$$+\,\mathcal{M}^{\mu}_{\pi^- p \to \omega n}(q,p,\lambda;\overline{q},\overline{p},\overline{\lambda})\,\mathcal{M}_{\omega \to e^+e^-\;\mu}(\overline{q};p_+,\lambda_+,p_-,\lambda_-). \quad (27)$$

The e^+e^- decay amplitudes include the vector meson propagators,

$$S_\rho(\overline{q}^2) \equiv \frac{1}{\overline{q}^2 - M_\rho^2 + i\Gamma_\rho(\overline{q}^2)\, M_\rho}, \tag{28}$$

$$S_\omega(\overline{q}^2) \equiv \frac{1}{\overline{q}^2 - M_\omega^2 + i\Gamma_\omega\, M_\omega}, \tag{29}$$

where the energy-dependent ρ-width is given by

$$\Gamma_\rho(\overline{q}^2) = \Gamma_\rho \, \frac{M_\rho}{\sqrt{\overline{q}^2}} \left(\frac{\overline{q}^2 - 4m_\pi^2}{M_\rho^2 - 4m_\pi^2} \right)^{\frac{3}{2}}, \tag{30}$$

Γ_ρ and Γ_ω denoting the widths at the peak of the ρ- and ω-resonances.

We perform the lepton sums and integrations and average over the angle between the initial and final 3-momenta. Using Eqs. (9) to (14), we find

$$\begin{aligned}
\left[\frac{d\sigma}{d\overline{q}^2}\right]_{\pi^- p \to e^+e^- n} = \; & \frac{\alpha}{6\pi^2} \frac{M_p\, M_n}{s} \frac{|\vec{p}|}{|\vec{p}|}\, m_e^2 (1 + \frac{\overline{q}^2}{2m_e^2})\, (1 - \frac{4m_e^2}{\overline{q}^2})^{\frac{1}{2}} \\
& \Bigg[\frac{f_\rho^2}{M_\rho^4}\; S_\rho^*(\overline{q}^2)\, S_\rho(\overline{q}^2)\; \sum_J \overline{C}_{JJ}\; M^{J*}_{\pi^- p \to \rho^0 n}(s)\, M^J_{\pi^- p \to \rho^0 n}(s) \\
& + \frac{f_\rho f_\omega}{M_\rho^2 M_\omega^2}\; S_\rho^*(\overline{q}^2)\, S_\omega(\overline{q}^2)\; \sum_J \overline{C}_{JJ}\; M^{J*}_{\pi^- p \to \rho^0 n}(s)\, M^J_{\pi^- p \to \omega n}(s) \\
& + \frac{f_\omega f_\rho}{M_\rho^2 M_\omega^2}\; S_\omega^*(\overline{q}^2)\, S_\rho(\overline{q}^2)\; \sum_J \overline{C}_{JJ}\; M^{J*}_{\pi^- p \to \omega n}(s)\, M^J_{\pi^- p \to \rho^0 n}(s) \\
& + \frac{f_\omega^2}{M_\omega^4}\, S_\omega^*(\overline{q}^2)\, S_\omega(\overline{q}^2) \sum_J \overline{C}_{JJ}\; M^{J*}_{\pi^- p \to \omega^0 n}(s)\, M^J_{\pi^- p \to \omega n}(s) \Bigg],
\end{aligned} \tag{31}$$

where the $\overline{C}_{JJ}$ coefficients depend on $\sqrt{s}$ and $\overline{q}^2$ and are given in the center of mass frame by the expressions,

$$\overline{C}_{\frac{1}{2}\frac{1}{2}} = \frac{(p^0 + M_p)\,(\overline{p}^0 + M_n)}{4M_n M_p} \Big(1 + \frac{|\vec{\overline{p}}|^2}{3\overline{q}^2}\Big), \tag{32}$$

$$\overline{C}_{\frac{3}{2}\frac{3}{2}} = \frac{(\overline{p}^0 + M_n)}{(p^0 + M_p)} \frac{|\vec{p}|^4}{2M_n M_p} \Big(1 + \frac{|\vec{\overline{p}}|^2}{3\overline{q}^2}\Big). \tag{33}$$

The derivation of the cross section in the other isospin channel, $\pi^+ n \to e^+ e^- p$, is completely similar, with the obvious replacement of $\mathcal{M}_{\pi^- p \to \rho^0 n\ \mu}$ and $\mathcal{M}_{\pi^- p \to \omega n\ \mu}$ by $\mathcal{M}_{\pi^+ n \to \rho^0 p\ \mu}$ and $\mathcal{M}_{\pi^+ n \to \omega p\ \mu}$.

4 Numerical results

This section is devoted to the discussion of the $\pi^- p \to e^+ e^- n$ and $\pi^+ n \to e^+ e^- p$ differential cross sections for values of the total center of mass energy $\sqrt{s}$ ranging from 1.5 GeV up to 1.8 GeV. We explore the dependence of the $\rho^0 - \omega$ interference pattern in the $e^+ e^-$ channel on $\sqrt{s}$ in this energy range, in particular in the vicinity of the ω-meson production threshold ($\sqrt{s}$=1.72 GeV).

We consider first the differential cross section defined by Eq. (31) for the $\pi^- p \to e^+ e^- n$ and the $\pi^+ n \to e^+ e^- p$ reactions. The magnitude of the 4-vector $\overline{q}$ is the invariant mass $\mathrm{m}_{e^+ e^-}$ of the $e^+ e^-$ pair.

The differential cross sections calculated using Eq. (31) for the $\pi^- p \to e^+ e^- n$ and the $\pi^+ n \to e^+ e^- p$ reactions at $\sqrt{s}$=1.5 GeV are shown in Figs. 7 and 8.

These figures illustrate very clearly the isospin effects discussed in Section 2. For the two reactions, the ω and ρ^0 contributions to the cross section are the same. The ρ^0-ω interference is destructive for the $\pi^- p \to e^+ e^- n$ reaction and constructive for the $\pi^+ n \to e^+ e^- p$ process. Consequently, the $\pi^- p \to e^+ e^- n$ differential cross section is extremely small in the range of invariant masses considered in this calculation (less than 10 nb GeV^{-2}). In contrast, the constructive ρ^0-ω interference for the $\pi^+ n \to e^+ e^- p$ reaction leads to a sizeable differential cross section (of the order of 0.15 μb GeV^{-2}).

This is a very striking prediction, linked to the resonant structure of the scattering amplitudes $M^{1/2}_{\pi N \to VN}$ and $M^{3/2}_{\pi N \to VN}$. At $\sqrt{s}$=1.5 GeV, the coefficients $\overline{C}_{\frac{1}{2}\,\frac{1}{2}}$ and $\overline{C}_{\frac{3}{2}\,\frac{3}{2}}$ are 1.12 and 0.02 GeV^2 respectively (for $e^+ e^-$ pair invariant masses of the order of 0.5 GeV). The smallness of $\overline{C}_{\frac{3}{2}\,\frac{3}{2}}$ is a consequence of the relative D-wave state in the initial pion-nucleon system implied by the spin 3/2 of the channel. From the values of the amplitudes displayed in Figs. 4 and 5, it is easy to see that the J=1/2 and J=3/2 contributions to the $\pi^- p \to e^+ e^- n$ and $\pi^+ n \to e^+ e^- p$ differential cross sections are of comparable magnitude. These cross sections reflect the couplings of both the N(1520) and N(1535) baryon resonances to the vector meson-nucleon channels. Data on differential cross sections for the $\pi^- p \to e^+ e^- n$ and $\pi^+ n \to e^+ e^- p$ reactions at $\sqrt{s}$=1.5 GeV would be very useful for making progress in the understanding of these couplings.

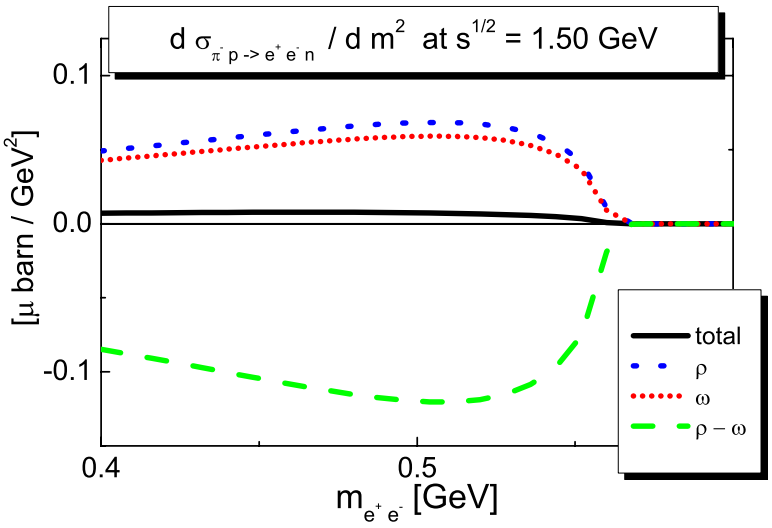

Fig. 7. Differential cross section for the $\pi^- p \to e^+ e^- n$ reaction at $\sqrt{s}$=1.5 GeV as function of the invariant mass of the e^+e^- pair. The ρ^0 and the ω contributions are indicated by short-dashed and dotted lines respectively. The long-dashed line shows the $\rho^0 - \omega$ interference. The solid line is the sum of the three contributions.

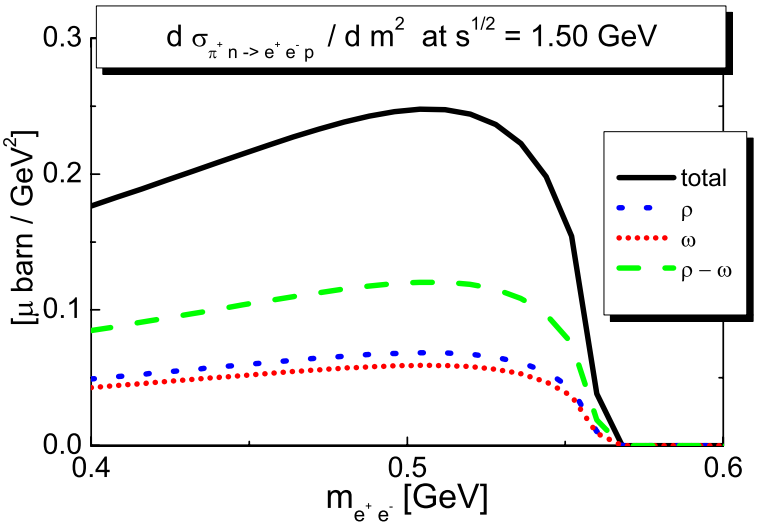

Fig. 8. Differential cross section for the $\pi^+ n \to e^+ e^- p$ reaction at $\sqrt{s}$=1.5 GeV as function of the invariant mass of the e^+e^- pair. The ρ^0 and the ω contributions are indicated by short-dashed and dotted lines respectively. The long-dashed line shows the $\rho^0 - \omega$ interference. The solid line is the sum of the three contributions.

The $\sqrt{s}$-dependence of the $\pi^- p \to e^+ e^- n$ differential cross section below the vector meson production threshold is illustrated in Figs. 9-11. The corresponding results for the $\pi^+ n \to e^+ e^- p$ reaction are shown in Figs. 12-14.

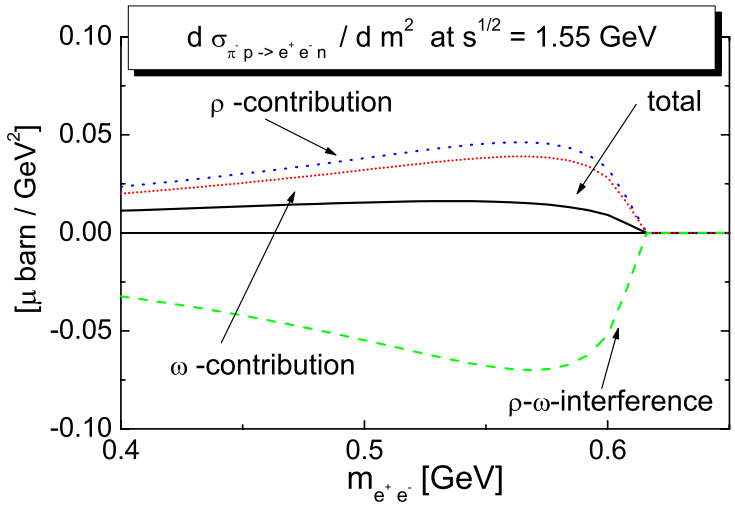

Fig. 9. Differential cross section for the $\pi^- p \to e^+ e^- n$ reaction at $\sqrt{s}$=1.55 GeV as function of the invariant mass of the $e^+ e^-$ pair.

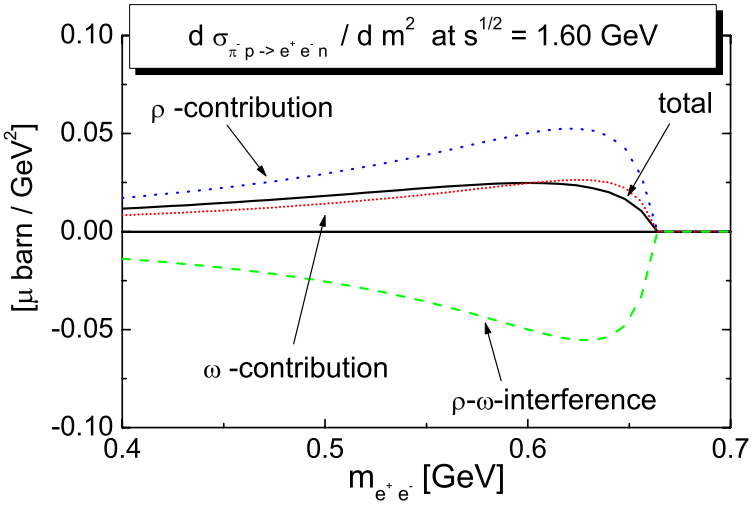

Fig. 10. Differential cross section for the $\pi^- p \to e^+ e^- n$ reaction at $\sqrt{s}$=1.60 GeV as function of the invariant mass of the $e^+ e^-$ pair.

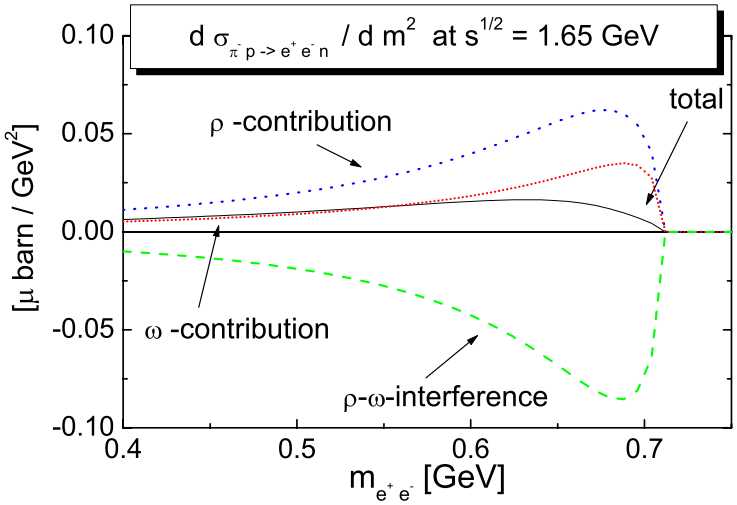

Fig. 11. Differential cross section for the $\pi^- p \to e^+e^- n$ reaction at $\sqrt{s}$=1.65 GeV as function of the invariant mass of the e^+e^- pair.

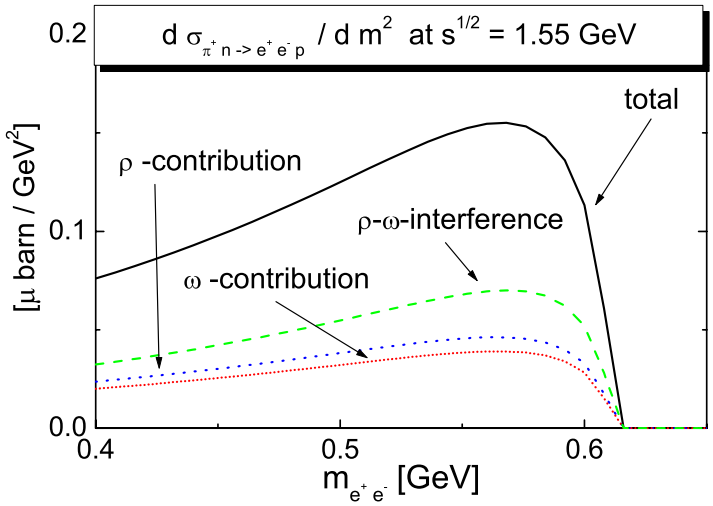

Fig. 12. Differential cross section for the $\pi^+ n \to e^+e^- p$ reaction at $\sqrt{s}$=1.55 GeV as function of the invariant mass of the e^+e^- pair.

These differential cross sections vary smoothly with the total center of mass energy. They exhibit the features discussed for $\sqrt{s}$=1.5 GeV. However they also reflect dynamics associated with higher-lying resonances [16]. We emphasize again that the relative s-wave assumed between the vector meson and the nucleon in the final state is appropriate only for values of $m_{e^+e^-}$ close to $(\sqrt{s} - M_N)$. The differential cross sections for the lowest e^+e^- pair invariant masses are expected to be outside the range of validity of the model of Ref. [16].

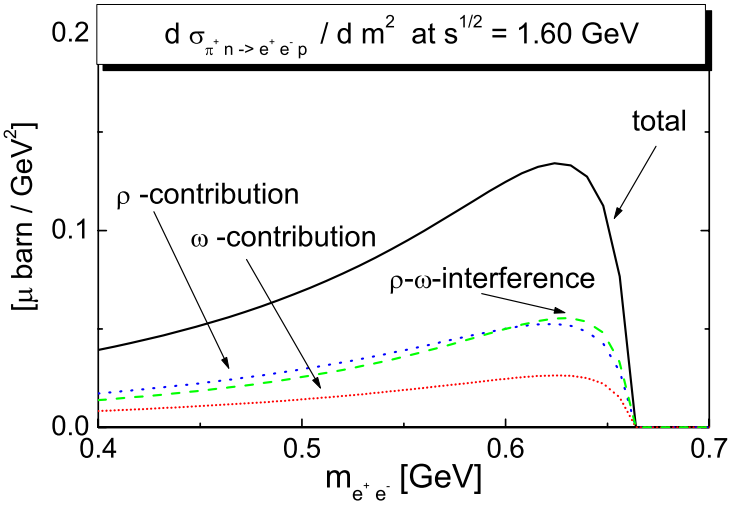

Fig. 13. Differential cross section for the $\pi^+ n \to e^+e^-p$ reaction at $\sqrt{s}$=1.60 GeV as function of the invariant mass of the e^+e^- pair.

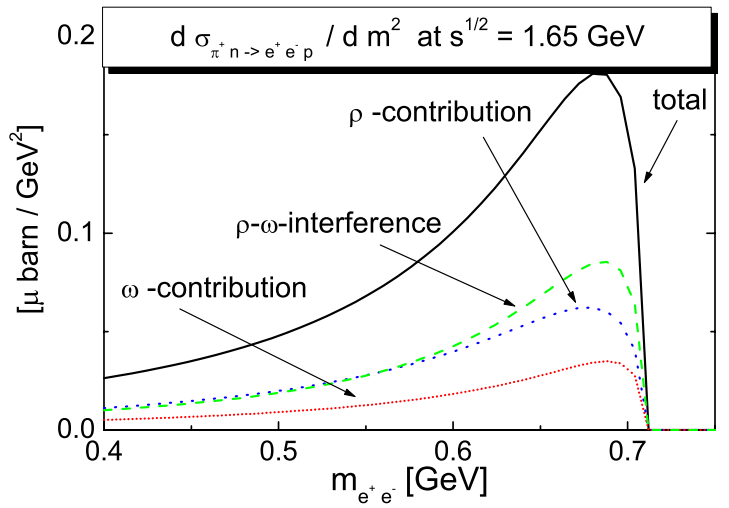

Fig. 14. Differential cross section for the $\pi^+ n \to e^+e^-p$ reaction at $\sqrt{s}$=1.65 GeV as function of the invariant mass of the e^+e^- pair.

The interference pattern changes drastically at the ω-meson threshold. This is shown in Figs. 15 and 16 for the $\pi^- p \to e^+e^-n$ differential cross section and in Figs. 17 and 18 for the $\pi^+ n \to e^+e^-p$ differential cross section.

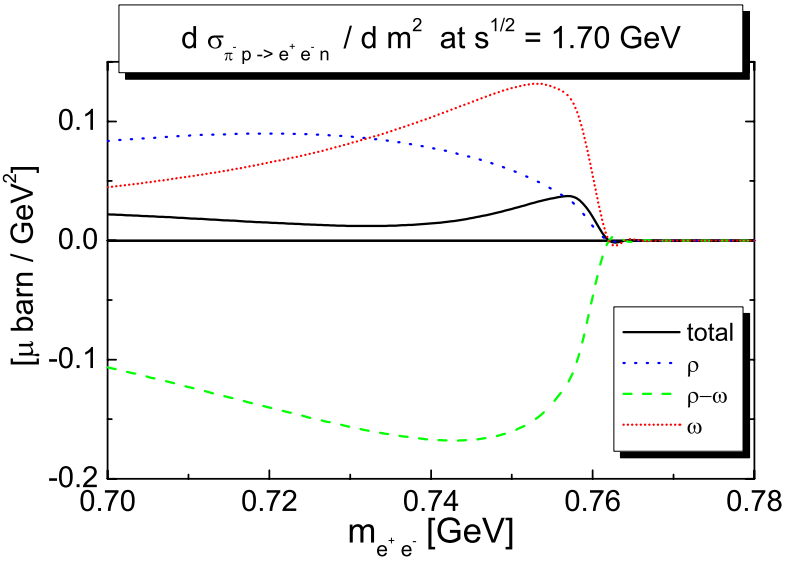

Fig. 15. Differential cross section for the $\pi^- p \to e^+ e^- n$ reaction at $\sqrt{s}$=1.70 GeV as function of the invariant mass of the e^+e^- pair.

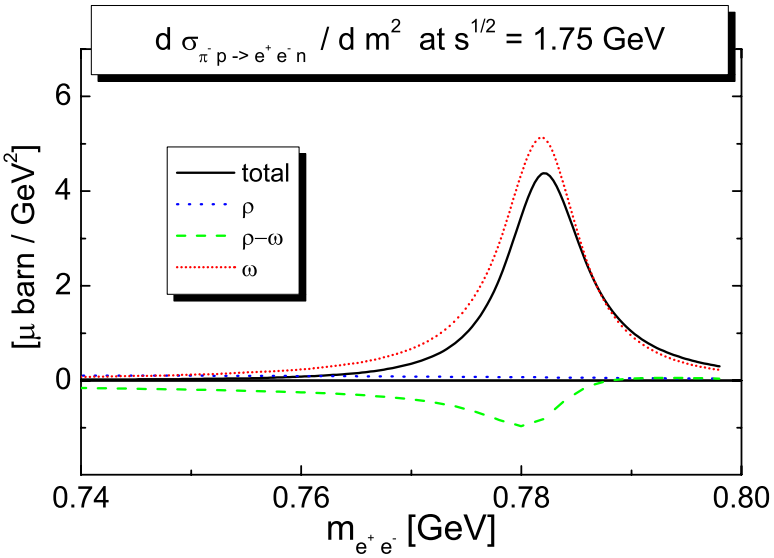

Fig. 16. Differential cross section for the $\pi^- p \to e^+ e^- n$ reaction at $\sqrt{s}$=1.75 GeV as function of the invariant mass of the e^+e^- pair.

Just below threshold, the ω-contribution begins to increase, while the general features of the e^+e^- production in the two isospin channels remain the same. Above the ω-meson production threshold, the differential cross sections for the $\pi^- p \to e^+ e^- n$ and $\pi^+ n \to e^+ e^- p$ reactions are completely dominated by the

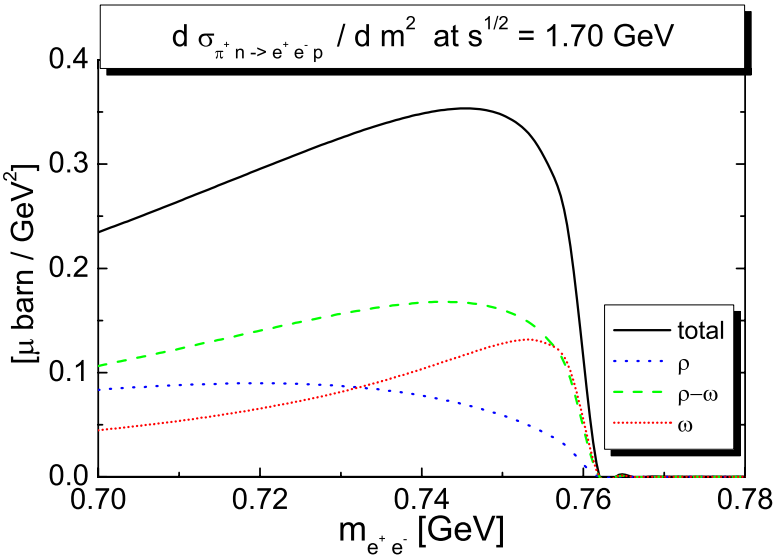

Fig. 17. Differential cross section for the $\pi^+ n \to e^+e^-p$ reaction at $\sqrt{s}$=1.70 GeV as function of the invariant mass of the e^+e^- pair.

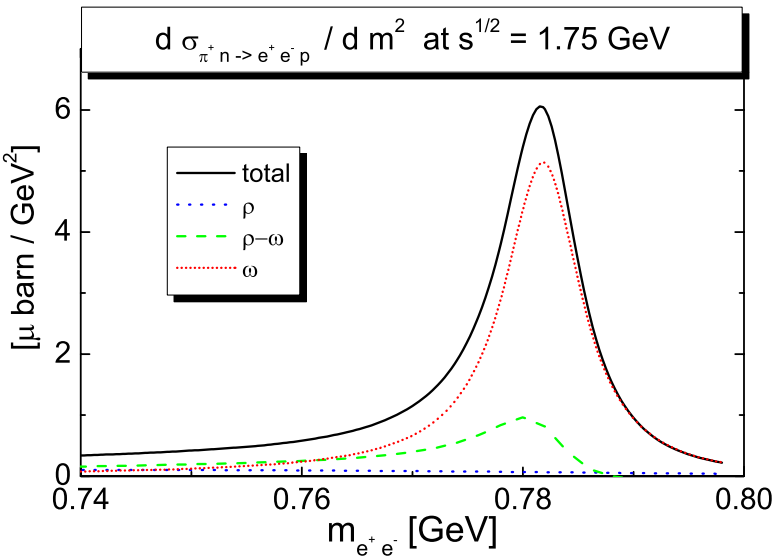

Fig. 18. Differential cross section for the $\pi^+ n \to e^+e^-p$ reaction at $\sqrt{s}$=1.75 GeV as function of the invariant mass of the e^+e^- pair.

ω-contribution. The magnitudes of the cross sections for the two reactions are comparable. The $\rho^0 - \omega$ interference is still destructive in the $\pi^- p \to e^+e^-n$ channel and constructive in the $\pi^+ n \to e^+e^-p$ channel, albeit very small. In both reactions, crossing the ω-production threshold leads to a sharp increase

in the cross section, by two orders of magnitude in the $\pi^- p \to e^+ e^- n$ channel and by one order of magnitude in the $\pi^+ n \to e^+ e^- p$ channel.

In order to see the s-channel resonant structure of the e^+e^- pair production more directly, it is interesting to look at the differential cross section as function of $\sqrt{s}$ for e^+e^- pairs of given invariant mass. This quantity is displayed in Fig. 19 for the $\pi^- p \to e^+ e^- n$ reaction and in Fig. 20 for the $\pi^+ n \to e^+ e^- p$ reaction. The invariant mass of the e^+e^- pair is 0.55 GeV. The structures associated with the N(1520) and N(1535) baryon resonances are particularly visible. In Figs. 21 and 22, we show differential cross sections as functions of $\sqrt{s}$ for e^+e^- pairs of invariant masses ranging from $m_{e^+e^-}$=0.40 GeV to 0.65 GeV. Our results are presented in Figs. 21 and 22 for the $\pi^- p \to e^+ e^- n$ and $\pi^+ n \to e^+ e^- p$ reactions respectively. The N(1650), the $\Delta(1620)$ and the $\Delta(1700)$ play a significant role in determining the cross sections for values of $\sqrt{s}$ close to the ω-meson production threshold.

It is interesting to compare our cross sections for the $\pi^- p \to e^+ e^- n$ and $\pi^+ n \to e^+ e^- p$ reactions with the recent work of Titov and Kämpfer [19]. In their approach, the $\pi N \to e^+ e^- N$ amplitudes are assumed to be dominated by s- and u-channel nucleon and baryon resonance exchanges. All baryon resonances with masses $\leq$1.72 GeV are included. The transition couplings of baryon resonances to vector fields are taken from the chiral quark model calculation of Riska and Brown [20]. The couplings to the ρN and ωN channels of the baryon resonances obtained in the hadronic theory of Ref. [16] are rather different from those obtained in the quark model of Ref. [20]. They are in general substantially weaker. This issue is discussed extensively in Ref. [16]. Consequently the $\pi^- p \to e^+ e^- n$ and $\pi^+ n \to e^+ e^- p$ cross sections are much larger in the calculation of Titov and Kämpfer but some trends are similar in both descriptions. At $\sqrt{s}$=1.6 GeV, the $\pi^+ n \to e^+ e^- p$ cross section is significantly larger than the $\pi^- p \to e^+ e^- n$ cross section. This reflects a constructive $\rho^0 - \omega$ interference in the first case and a destructive $\rho^0 - \omega$ interference in the latter process as in our approach. Much of the strength is provided by the S_{11} resonances. At $\sqrt{s}$=1.8 GeV, the cross sections for both reactions are comparable and dominated by the ω-contribution. The sensitivity of the $\pi^- p \to e^+ e^- n$ and $\pi^+ n \to e^+ e^- p$ cross sections to the strength of the transition couplings of baryon resonances to vector fields is the key result of both calculations. The magnitude of these cross sections below threshold would therefore provide very valuable information on vector meson-nucleon dynamics. The sensitivity of the $\pi^- p \to e^+ e^- n$ cross section to the couplings of baryon resonances to vector meson-nucleon channels can also be seen from a previous computation [21] we did in the same coupled-channel framework as the present calculation. In Ref. [21], the $\pi^- p \to \rho^0 n$ and $\pi^- p \to \omega n$ amplitudes were obtained without systematic constraints from meson photoproduction data. This led to very different couplings, in particular of the N(1520) to the $\rho^0 N$ channel, and to a constructive rather than a destructive $\rho^0 - \omega$ interference.

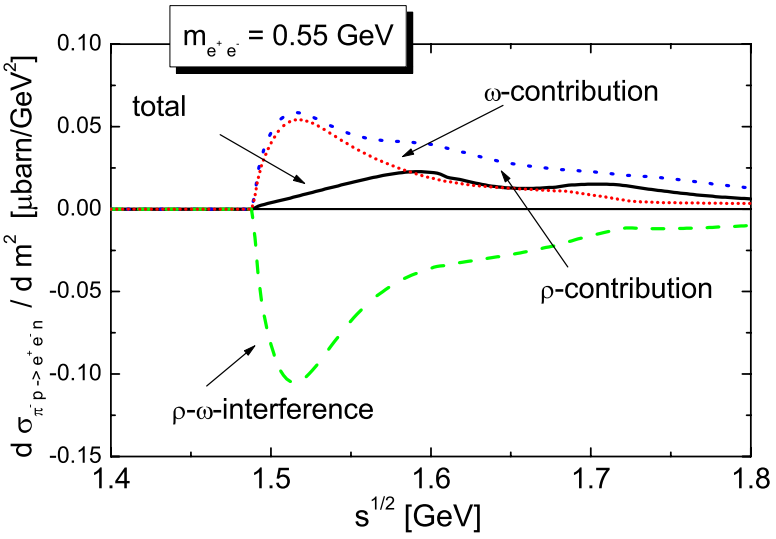

Fig. 19. Differential cross section for the $\pi^- p \to e^+e^- n$ reaction as function of the total pion-nucleon center of mass energy $\sqrt{s}$ for e^+e^- pairs of invariant mass $m_{e^+e^-}$=0.55 GeV.

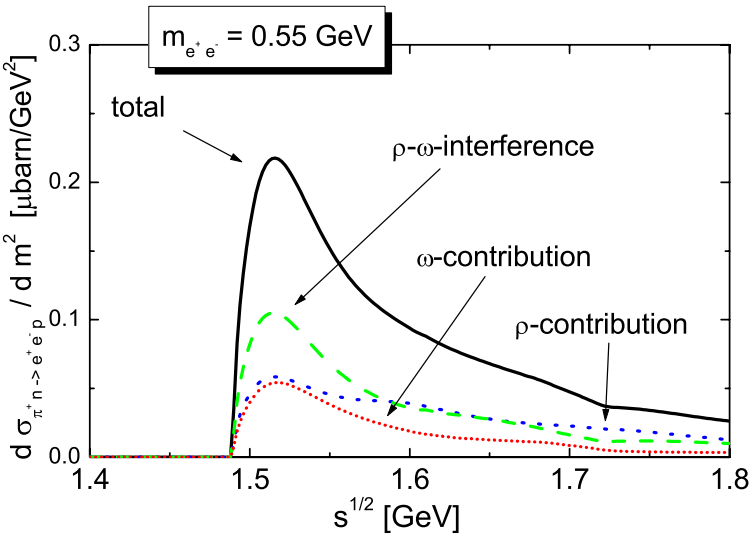

Fig. 20. Differential cross section for the $\pi^+ n \to e^+e^- p$ reaction as function of the total pion-nucleon center of mass energy $\sqrt{s}$ for e^+e^- pairs of invariant mass $m_{e^+e^-}$=0.55 GeV.

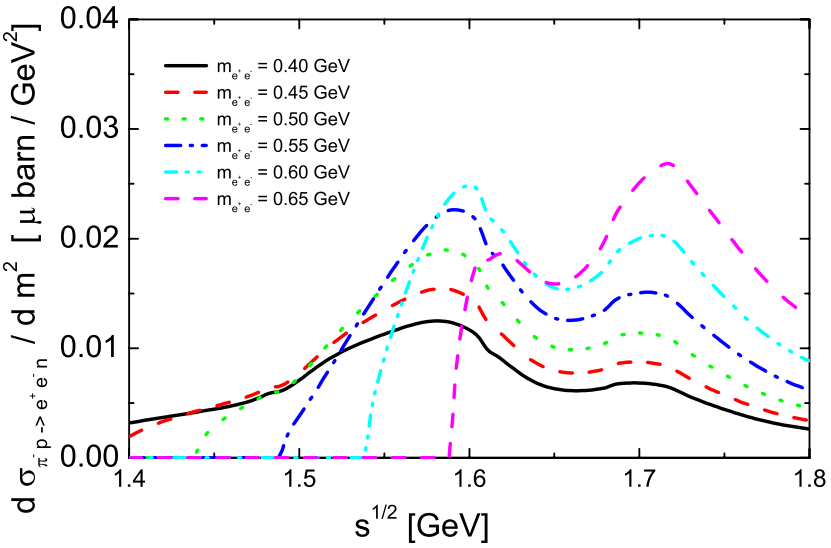

Fig. 21. Differential cross section for the $\pi^- p \to e^+ e^- n$ reaction as function of the total pion-nucleon center of mass energy $\sqrt{s}$ for e^+e^- pairs of invariant masses ranging from 0.40 until 0.65 GeV.

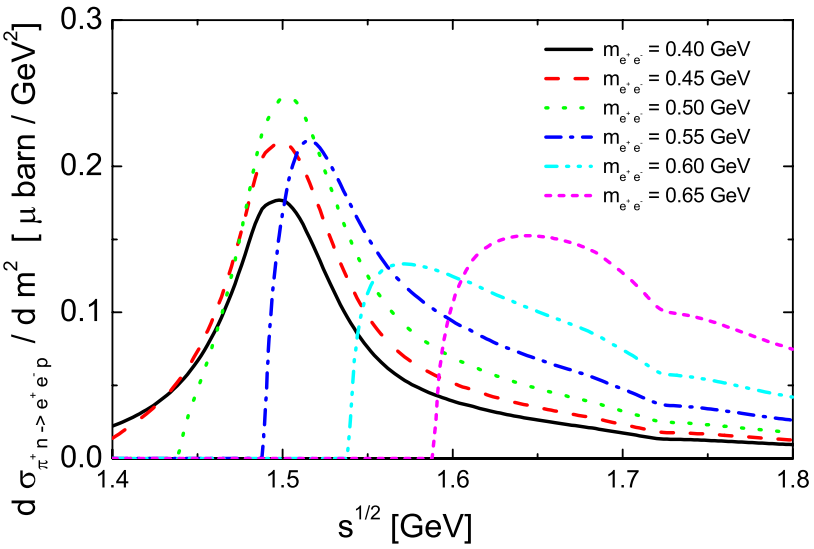

Fig. 22. Differential cross section for the $\pi^+ n \to e^+ e^- p$ reaction as function of the total pion-nucleon center of mass energy $\sqrt{s}$ for e^+e^- pairs of invariant masses ranging from 0.40 until 0.65 GeV.

5 Conclusion

We have computed the e^+e^- pair invariant mass distributions for the $\pi^- p \to e^+e^- n$ and $\pi^+ n \to e^+e^- p$ reactions below and close to the vector meson production threshold ($\sqrt{s}$=1.72 GeV).

We employ the $\pi N \to \rho^0 N$ and $\pi N \to \omega N$ amplitudes obtained in a recent relativistic and unitary coupled-channel approach to meson-nucleon scattering [16]. This description reproduces a large body of data on pion-nucleon elastic and inelastic scattering and on meson photoproduction off nucleons in the energy range $1.4 < \sqrt{s} < 1.8$ GeV. In the model, pion-nucleon resonances are generated dynamically and the coupling strengths of these resonances to vector meson-nucleon channels are predicted. These couplings are not well-known.

Using the Vector Meson Dominance assumption, we have shown that the differential cross sections for the $\pi^- p \to e^+e^- n$ and $\pi^+ n \to e^+e^- p$ reactions below the ω-threshold are very sensitive to the coupling of low-lying baryon resonances to vector meson-nucleon final states. We find that the $\rho^0 - \omega$ interference is destructive in the $\pi^- p \to e^+e^- n$ channel and constructive in the $\pi^+ n \to e^+e^- p$ channel. We predict a very small cross section for the $\pi^- p \to e^+e^- n$ reaction below threshold and a sizeable cross section for the $\pi^+ n \to e^+e^- p$ reaction in this energy range. Above the ω-meson production threshold, both cross sections are comparable and much larger.

The magnitude of the $\pi^- p \to e^+e^- n$ and $\pi^+ n \to e^+e^- p$ differential cross sections below the ω-threshold depends strongly on the structure and dynamics of baryon resonances. These reactions deserve experimental studies. Such a programme could be carried at GSI (Darmstadt) using the available pion beam and the HADES spectrometer [9]. These measurements would provide a necessary step towards the understanding of e^+e^- pair production in pion-nucleus reactions and in general significant constraints on the propagation of vector mesons in the nuclear medium.

References

[1] R.A. Arndt et al., Phys. Rev. C 52 (1995) 2120.

[2] R.A. Arndt et al., nucl-th/9807087.

[3] D.M. Manley and E.M. Saleski, Phys. Rev. D 45 (1992) 4002.

[4] T.P. Vrana, S.A. Dytman and T.-S.H. Lee, Phys. Rep. 328 (2000) 181.

[5] G.E. Brown and M. Rho, Phys. Rev. Lett. 66 (1991) 2720.

[6] R. Rapp and J. Wambach, Adv. Nucl. Phys. 25 (2000) 1.

[7] W. Schön et al., Acta Physica Polonica B 27 (1996) 2959.

[8] M. Effenberger et al., Phys. Rev. C 60 (1999) 027601.

[9] HADES Collaboration, private communication.

[10] H. Alvensleben et al., Nucl. Phys. **B 25** (1971) 33.

[11] J.J. Sakurai, Currents and Mesons, The University of Chicago Press, 1969.

[12] N.M. Kroll, T.D. Lee and B. Zumino, Phys. Rev. 157 (1967) 1376.

[13] R.W. Gothe, D. Wacker and B. Schoch, Acta Physica Polonica B 29 (1998) 3313.

[14] B. Krusche, Acta Physica Polonica B 29 (1998) 3335; Hirschegg 2001 Proceedings, Structure of Hadrons, Hirschegg (Austria), January 14th-20th, 2001, p. 162.

[15] J.J. Manach et al., Nucl. Phys. A 663 (2000) 671*c*; M. Battaglieri et al., hep-ex/0107028.

[16] M.F.M. Lutz, Gy. Wolf and B. Friman, nucl-th/0112052.

[17] M.F.M. Lutz and E.E. Kolomeitsev, nucl-th/0105042, Nucl. Phys. A. in press.

[18] B. Friman and M. Soyeur, Nucl. Phys. A 600 (1996) 477.

[19] A.I. Titov and B. Kämpfer, Eur. Phys. J. A. 12 (2001) 217.

[20] D.O. Riska and G.E. Brown, Nucl. Phys. A 679 (2001) 577.

[21] M. Soyeur, M.F.M. Lutz and B. Friman, Proceedings of the International Workshop XXVIII on Gross Properties of Nuclei and Nuclear Excitations, Hirschegg, Austria, January 16-22, 2000.